Article

Cancer Cell

Dual Targeting of the Autophagic Regulatory Circuitry in Gliomas with Repurposed Drugs Elicits Cell-Lethal Autophagy and Therapeutic Benefit

Graphical Abstract

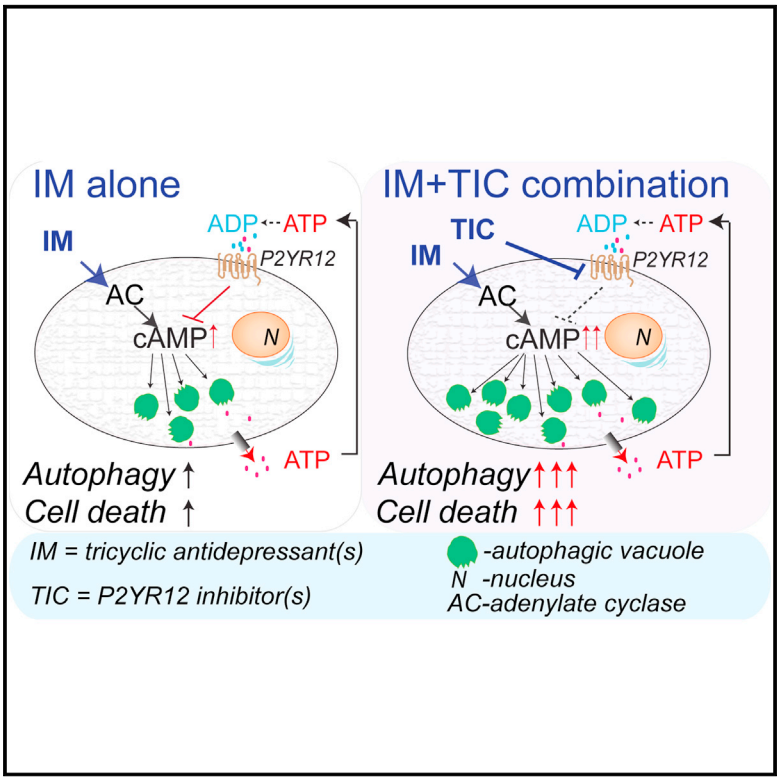

Authors

Ksenya Shchors, Aristea Massaras, Douglas Hanahan

Correspondence

douglas.hanahan@epfl.ch

In Brief

Shchors et al. show that combinatorial treatment with tricyclic antidepressants and a subclass of anticoagulants targeting $P2RY_{12}$ halts glioma progression in pre-clinical models by evoking hyperactive levels of autophagy and cell death.

Highlights

- Tricyclic antidepressants plus $P2Y_{12}$ inhibitors coordinately elicit death in glioma
- Dual therapy with autophagy enhancers impairs glioma progression
- By elevating cAMP levels via distinct mechanisms, IM and TIC increase autophagic flux

Shchors et al., 2015, Cancer Cell *28*, 456–471
October 12, 2015
http://dx.doi.org/10.1016/j.ccell.2015.08.012

CellPress

CellPress

Cancer Cell
Article

Dual Targeting of the Autophagic Regulatory Circuitry in Gliomas with Repurposed Drugs Elicits Cell-Lethal Autophagy and Therapeutic Benefit

Ksenya Shchors,[1] Aristea Massaras,[1] and Douglas Hanahan[1,*]
[1]Swiss Institute for Experimental Cancer Research, Swiss Federal Institute of Technology, Lausanne 1015, Switzerland
*Correspondence: douglas.hanahan@epfl.ch
http://dx.doi.org/10.1016/j.ccell.2015.08.012

SUMMARY

The associations of tricyclic antidepressants (TCAs) with reduced incidence of gliomas and elevated autophagy in glioma cells motivated investigation in mouse models of gliomagenesis. First, we established that imipramine, a TCA, increased autophagy and conveyed modest therapeutic benefit in tumor-bearing animals. Then we screened clinically approved agents suggested to affect autophagy for their ability to enhance imipramine-induced autophagy-associated cell death. The anticoagulant ticlopidine, which inhibits the purinergic receptor $P2Y_{12}$, potentiated imipramine, elevating cAMP, a modulator of autophagy, reducing cell viability in culture, and increasing survival in glioma-bearing mice. Efficacy of the combination was obviated by knockdown of the autophagic regulatory gene ATG7, implicating cell-lethal autophagy. This seemingly innocuous combination of TCAs and $P2Y_{12}$ inhibitors may have applicability for treating glioma.

INTRODUCTION

High-grade astrocytomas (anaplastic astrocytoma grade III [AA] and glioblastoma [GBM]) have the highest incidence and mortality rate among primary brain cancer patients (Friedman et al., 2000); survival benefits from current therapies are measured in months. The identification of new mechanism-based therapeutic targets and strategies that improve upon this bleak outlook is an important agenda.

In recent years, the roles of catabolic recycling of cellular components (autophagy) in malignant progression and in responses to therapy have become a focus in glioma, and other cancers. Although in some cases autophagy exhibits pro-tumorigenic effects (Hart et al., 2012), in gliomas autophagy has been suggested to inhibit tumor progression and to potentiate responses to conventional therapies (Aoki et al., 2008; Palumbo and Comincini, 2013). In the present study, we evaluated the mechanistic effects and therapeutic potential of manipulating autophagy in gliomas using repurposed USA Food and Drug Administration (FDA)-approved agents.

RESULTS

Imipramine Treatment Prolongs Survival of Glioma-Bearing Animals

Long-term use of tricyclic antidepressants (TCAs) has been associated with decreased incidence of gliomas (Walker et al., 2011). Intrigued by this observation, we asked whether TCA treatment might affect the progression of pre-existing low-grade lesions to secondary GBMs in genetically engineered mouse models of gliomagenesis. We and others have previously established that p53 deficiency promotes the formation of high-grade gliomas in animals expressing activated $HRas^{V12}$ oncogene (Marumoto et al., 2009; Shchors et al., 2013). For this study, we generated two lines of mice, differing in their p53 status: *GFAP*-$HRas^{V12}$;*GFAP-CRE*;*GFAP-LUC*;$p53^{flox/wt}$ (referred to here as *GRLp53het* mice) and *GFAP-*$HRas^{V12}$;*GFAP-CRE*;*GFAP-LUC*;$p53^{flox/flox}$ (*GRLp53fko*). The homozygous loss of p53 in this context significantly accelerated the progression of high-grade gliomas when compared with p53 heterozygous animals (Figure S1A) (Shchors et al., 2013). These mice

Significance

Glioma, a form of brain cancer, remains an intractable disease, for which standard-of-care treatments are largely inadequate. Discovering new therapeutic strategies to combat gliomas is therefore an important agenda. We describe a means to impair glioma growth and malignant progression by increasing autophagic flux upon combining two classes of clinically approved drugs: tricyclic antidepressants (TCAs) and certain anticoagulants. We show that combining a TCA and an inhibitor of the purinergic receptor $P2Y_{12}$ promotes autophagy-associated cell death in glioma cells via the EPAC branch of the cAMP-signaling pathway. Pre-clinical trials in several models of glioma development and progression demonstrate therapeutic efficacy. Thus, combinations of TCAs and $P2Y_{12}$ inhibitors could be considered for clinical evaluation as an adjuvant to conventional glioma therapy.

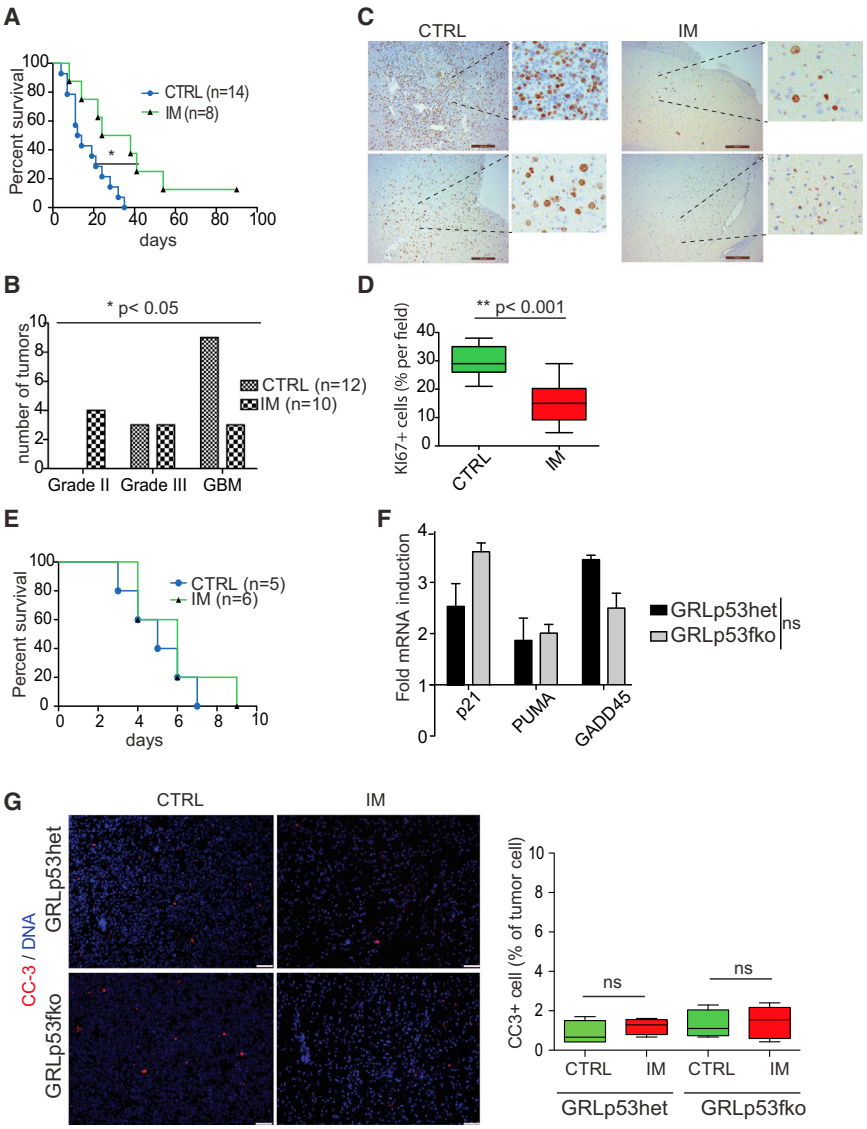

Figure 1. IM Treatment Improves Survival and Decreases Malignancy in Engineered Mouse Models of De Novo Gliomagenesis

(A) Kaplan-Meier survival analysis of tumor-bearing *GRLp53het* animals in cohorts treated with vehicle control (CTRL) or with IM (40 mg/kg/day). Treatment was initiated 24 hr after tumor detection (see Experimental Procedures). *p < 0.02 by the Mantel-Cox test.

(B) The distribution of grade II, III, and IV tumors in end-stage GRLp53het mice, control (CTRL) and treated with IM. The histopathological score was determined as described in the Supplemental Information. Statistical analysis was performed using the chi-square test.

(C) Representative images of an IHC analysis of cell proliferation in *GRLp53het* tumors, control (CTRL) and treated with IM, assayed for Ki67 (see Supplemental Information). The scale bars represent 200 μm; insets are magnified 14×. **p < 0.001 by unpaired Student's t test.

(E) Survival of tumor-bearing *GRLp53fko* animals in a control group (CTRL) or one treated with IM. Treatment began 24 hr after tumor detection (as in A). The size of each cohort is indicated. No statistically significant difference was detected by the Mantel-Cox test.

(F) RT-qPCR analysis of mRNA expression of the p53 target genes: *CDKN1a* (*p21cip1*), *puma*, and *gadd45a* in tumor-derived primary cultures from *GRLp53het* and *GRLp53fko* animals following 24 hr of exposure to IM in vitro. Data are presented as fold induction relative to control vehicle-treated samples. Ns, no statistical significance by two-way ANOVA. Three independently derived tumor cultures were analyzed, each in triplicate.

(G) Representative images from an IHC analysis of apoptosis assayed by activated caspase-3 (CC-3) staining in brains collected from *GRLp53het* and *GRLp53fko* mice, control or treated with IM for 72 hr (see Supplemental Information). The scale bars represent 50 μm. Quantification of CC3-positive cells in tumor fields is presented to the right. Statistical analysis was performed using a two-tailed Student's t test.

See also Figure S1.

reproducibly develop high-grade astrocytomas (AA and GBM-like lesions) (Figure S1). The tumors developing in the *GRLp53het* and *GRLp53fko* animals varied in histopathological grade, with the *GRLp53fko* model having a higher incidence of the GBM-like tumors (80% versus 59% in the *GRLp53het* model) (Figure S1B). The molecular alterations detected in GBMs from the *GFAP-HRas*^{V12}-driven model of gliomagenesis are similar to those observed in a range of high-grade human gliomas, including overexpression of EGF receptor and increased activity of the AKT/mTOR signaling pathway (Shannon et al., 2005) (Figure S1C). The incorporation of a luciferase reporter enables non-invasive monitoring of disease progression (Figures S1G–S1J and Supplemental Information).

We first assessed the impact on tumor-bearing *GRLp53het* animals of a TCA, imipramine (IM). Asymptomatic *GRLp53het* animals with similarly sized incipient gliomas were stratified into control and IM-treated cohorts. The IM cohort (5 days/week) was treated until a defined endpoint 13 weeks later or until the effects of tumor progression dictated euthanasia. The IM treatment prolonged the overall survival of treated animals, with a median survival of 31 days compared with 13 days in the control cohort (Figure 1A). The IM-treated tumors exhibited a lower histopathological grade and had a reduced proliferative index, as assessed by Ki67, compared with the control group; only 36% of treated mice had progressed to high-grade GBM-like lesions, versus 75% in the control cohort (Figures 1B–1D). In contrast, when *GRLp53fko* mice (which exhibit accelerated tumor progression) (Figure S1A) were similarly selected and treated with IM, there was no survival advantage (Figure 1E). Thus, IM treatment was able to delay the progression of incipient low-grade gliomas but not the more aggressive disease. The differential sensitivity of *GRLp53het* and *GRLp53fko* lesions to IM treatment was independent of transcriptional activation of p53 targets (Figure 1F).

To understand the basis for the therapeutic efficacy of IM against low-grade gliomas, we examined the effects of IM action in tumors as well as cultured glioma cells of mouse and human origin. It has been suggested, depending on the context, that TCAs disrupt tumor cell homeostasis via several mechanisms, including accentuated autophagy, alterations in lysosomal turnover, and elevated apoptosis (Jahchan et al., 2013; Jeon et al., 2011; Petersen et al., 2013). Analysis of tumor samples collected from *GRLp53het* and *GRLp53fko* control and IM-treated animals did not reveal a heightened frequency of apoptosis in the gliomas treated with IM (Figure 1G). Therefore, we focused on the implication that IM could be modulating autophagy (Jeon et al., 2011).

The process of autophagy involves multiple stages. Following initiation, evidenced by autophagosome formation, the process can either become stalled at a midpoint (non-functional) or be productive (functional) at completing the degradation of enveloped cellular organelles, termed autophagic flux. A common metric for the initiation of autophagy involves the microtubule-associated protein light chain 3 (MAP1 LC3, hereafter referred to as *LC3*). The conversion of cytosolic LC3I into phosphatidylethanolamine-conjugated LC3II closely correlates with the number of autophagosomes in the cell and is manifested as puncta by immunohistochemical (IHC) analysis or as a faster migrating LC3 isoform in SDS-PAGE (Mizushima et al., 2010). Tumor samples were collected from symptomatic tumor-bearing *GRLp53ko* animals, subjected to IM or control-vehicle treatment for 72 hours, and analyzed for LC3 expression. We detected an increase in the abundance of LC3-II puncta per cell in tumors collected from the IM-treated animals compared with control tumors (mean ± SEM 3.174 ± 0.56 and 1.088 ± 0.35, respectively), as well as an increase in the LC3II isoform visualized by SDS-PAGE in tumor lysates and primary glioma cells derived from the *GRLp53fko* and *GRLp53het* mice and in human GBM cell lines (Figures 2A–2D). This effect was not associated with altered transcriptional regulation of LC3 (Figure 2E).

During the final stages of the autophagic process, the LC3-II protein is degraded in autolysosomes. Pharmacological inhibition of LC3-II degradation in lysosomes is used as a metric of productive autophagic flux (Mizushima et al., 2010). Indeed, an inhibitor of lysosomal acidification, Bafilomycin A1 (Baf1), was found to promote LC3 accumulation in IM-treated glioma cells (Figure 2F), indicating that it was otherwise being degraded in the end stage of autophagy.

A Cell-Based Screen for Drugs that Enhances IM's Effects on Autophagy and Cell Survival

IM exposure interfered with the progression of low-grade incipient neoplasia in *GRLp53het* mice but was ineffective in *GRLp53fko* mice exhibiting more rapid disease progression (Figures 1A and 1E). Similarly, in a cohort of human glioma patients, in which high-grade glioma patients were overrepresented, post-diagnostic treatment with TCAs produced very limited survival benefits (Walker et al., 2012). We reasoned that IM's modest activity in high-grade gliomas could be potentially enhanced in terms of therapeutic benefit by a combinatorial approach. Given that we (Figure 2) and others (Jeon et al., 2011) observed that IM modulates autophagic flux in this cell type, we screened for agents that could intensify IM-mediated regulation of autophagy and enhance its anti-tumoral activity in glial cells. Notably, other clinically approved drugs have recently been revealed to modulate autophagy by affecting different stages or regulators of this process (Hundeshagen et al., 2011; Williams et al., 2008). We evaluated a set of agents that were implicated to modulate autophagy at distinctive nodes (Figure 3A), focusing on drugs that were not associated with significant side effects in humans (Table S1).

We tested the effects of the selected drugs, alone and in combination with 20 or 40 μM IM, on cell survival in a panel of six human glioma cells lines differing in PTEN, p53, and $INK4^{ARF}$ status. Proliferation and survival were measured 72 hours following exposure (Figure S2A). The maximum tested dose of each drug was based upon its highest non-toxic concentration in plasma of human patients. Only one of the tested agents, the anti-platelet drug ticlopidine (TIC), synergized with IM in reducing cell survival in all tested lines (independent of the activity of the AKT/mTOR signaling pathway and of EGF receptor levels) (Figure S2B). The combination was also effective in primary GBM cultures derived from the *GRLp53het* and *GRLp53fko* mice and had minimal toxicity toward normal mouse astrocytes in vitro (Figures 3B, S2A, S2C, and S3A).

TIC inhibits the ADP receptor $P2Y_{12}$, thereby abolishing the ADP-induced downregulation of adenylyl cyclase. In normal tissue, expression of $P2Y_{12}$ is limited to platelets and glial cells. In gliomas, $P2Y_{12}$ is expressed at higher levels in cancer cells than in normal astrocytes (Barańska et al., 2004; Carrasquero et al., 2005) (Figure S3B). Concordantly, $P2Y_{12}$ was elevated in *GRLp53het* gliomas cells compared with wild-type astrocytes and was detected in all tested human glioma cell lines (Figure S3C).

We hypothesized that inhibition of $P2Y_{12}$ activity in conjunction with TCA treatment was increasing the cellular level of cAMP by upregulating adenylate cyclase (Hollopeter et al., 2001; Toki et al., 1999), which in turn elevates the rate of autophagic flux (Ugland et al., 2011) (Figure 3C). If indeed IM and TIC act by targeting Gα and $P2Y_{12}$ respectively, then other chemically distinct drugs targeting these proteins should have similar combinatorial effects in gliomas. Therefore, we analyzed two additional TCAs, desipramine (DMI) and trifluoperazine (TFP), and two additional $P2Y_{12}$ inhibitors, prasugrel (PGL) and clopidogrel (CDL), alone and in combination, for their ability to reduce survival of glioma cells. All of the analogous combinations of a TCA and a $P2Y_{12}$ inhibitor synergistically reduced the survival of glioma cells to varying degrees, strengthening the conclusion that IM+TIC treatment was elevating cAMP (Figure 3D). Among the agents tested, DMI was more potent in inducing cell death in vitro compared with IM, and the $P2Y_{12}$ inhibitor CDL was similarly efficacious to TIC (Figure 3D). Beyond the immediate result of target validation, DMI and CDL warrant future evaluation as therapeutic agents.

Having established that drug combinations targeting the autophagic regulatory circuitry reduced cell survival (Figures 3B, 3D, and 3E), we next sought to characterize the mechanism of cell death. With regard to apoptosis, we found that the reduced survival of LN71 glioma cells treated with IM+TIC was not associated with the cleavage of the caspase-3 target protein poly ADP ribose polymerase (PARP), suggesting that IM+TIC treatment induces non-apoptotic cell death in LN71 cultured glioma cells (Figure 3F). Congruent with this observation, the

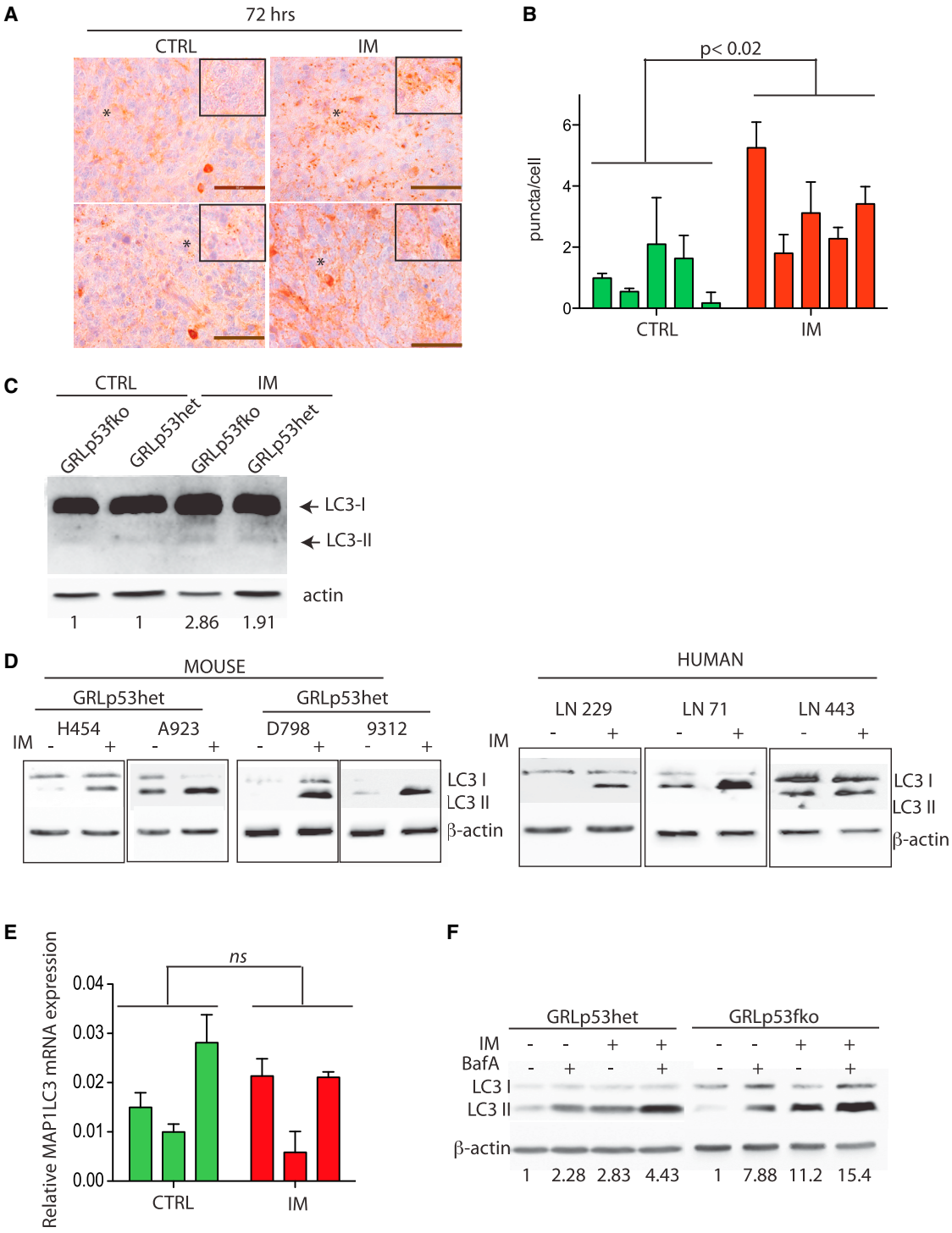

Figure 2. IM Treatment Induces Autophagy in Human and Mouse Glioma Cells

(A) Representative IHC analysis of LC3 expression and distribution in tumors collected from control (CTRL) and animals treated with IM for three days (see Supplemental Information). The scale bars represent 50 μm. Insets are magnified 8×.

(B) Quantification of LC3II puncta/cell in tumors described above. Statistical analysis was done by unpaired Student's t test.

(C) Immunoblotting analysis of LC3 expression in *GRLp53het* and *GRLp53fko* tumors collected from control and IM-treated animals treated as described above. Quantification of LC3 levels in treated animals relative to the respective controls is presented below the immunoblot.

(D) Immunoblotting analysis of LC3 expression in mouse and human glioma cells, either control (sham-treated) (-) or IM treated (+) for 24 hr. Independently derived primary cell lines from the *GRLp53het* (H454, A923) and *GRLp53fko* (D798, 9312) animals and human GBM cell lines (LN229, LN71, LN 443) were treated.

(legend continued on next page)

pan-caspase inhibitor Z-VAD-(0Me)-fmk failed to protect glioma cells from the IM+TIC-induced cell death (Figures 3G and 3H). In some experimental systems, IM has been implicated as an inhibitor of autophagy that acts by increasing lysosome membrane permeability, thereby causing an increase in apoptosis (Ashoor et al., 2013; Petersen et al., 2013). The lack of detectable apoptosis and the elevated autophagic flux (further described below) seen in the IM-treated glioma cells suggest that the reported ability of IM to inhibit rather than accentuate autophagy is not operative in this particular cancer cell type. In addition, the inhibition of necroptosis (programmed cell death by necrosis) by necrostatin-1 (25 μM), a small-molecular inhibitor of necroptosis (Degterev et al., 2005), did not block IM+TIC-induced cell death (Figures 3I and 3J).

Having excluded apoptosis and necroptosis as major determinants of the induced cell death, we proceeded to evaluate the role of heightened rates of autophagy in reducing survival of cultured glioma cells. A number of studies suggest that increases in cellular autophagy in vitro and in vivo can promote non-apoptotic cell death (for reviews, see Jain et al., 2013; Tsujimoto, 2012). To determine whether IM+TIC was also modulating the rate of cellular autophagy, as observed for IM treatment (Figure 2A), we first analyzed expression of LC3-II in LN71 glioma cells mock-treated or treated with IM, TIC, or IM+TIC. Indeed, IM+TIC treatment further enhanced LC3-II levels compared with IM or TIC (Figure 4A).

Autophagy is a dynamic, multi-stage process. The elevated levels of LC3-II reflect the initiation of the autophagic process but not necessarily its completion; as such, elevated LC3-II can be indicative of an increase in autophagy or, alternatively, stalling midcourse. To distinguish between these possibilities, we performed immunoblotting analysis of the cellular levels of p62/SQSTM1, which is known to recognize damaged proteins and shepherd them in autolysosomes, where p62 is concomitantly degraded. As such, cellular levels of p62/SQSTM1 reflect the status of autophagic flux in the cell (Bjørkøy et al., 2009; Pankiv et al., 2007). The levels of p62/SQSTM1 in LN71 glioma cells treated with IM+TIC were found to be significantly reduced compared with control, indicative of increased rates of functional autophagy (Figure 4A). Both Baf1 and the lysosomotropic reagent chloroquine (CQ) inhibited degradation of LC3-II in IM+TIC-treated samples (Figures 4B and 4C). The observed changes in the MAP1LC3 and p62/SQSTM1 protein levels in response to IM, TIC, and IM+TIC treatments were not a result of transcriptional regulation (Figure S3D), consistent with a direct effect on the autophagic machinery. Moreover, CQ treatment partially impedes IM+TIC-induced cell death (Figure S3F), further indicating that IM+TIC accentuates autophagy.

To further evaluate the outcome of IM+TIC treatment on glioma cells, we used a mRFP-EGFP-LC3 *tandem*-tagged fluorescent protein (p*tf-LC3*) (Kimura et al., 2007). EGFP is sensitive to lysosomal proteolysis, while red fluorescent protein (mRFP) retains fluorescence in autolysosomes. Therefore, ptfLC3 allows one to measure both induction of autophagy (mRFP+EGFP positive puncta) and productive autophagic flux reflected in an increase in the percentage of mRFP-only positive vehicles. A 48 hr IM+TIC treatment of LN71 glioma cells transfected with ptfLC3 resulted in an increase in red-only fluorescent vesicles compared with $mRFP^{+}EGFP^{+}$ puncta (Figure 4D), indicative of EGFP proteolysis in lysosomes, consistent with the other data indicating that the combination IM+TIC is promoting functional autophagy in glioma cells.

To substantiate this conclusion, we interfered with the expression of two key autophagic regulatory genes, *Beclin-1* and *ATG-7*. Small hairpin RNA (shRNA)-mediated downregulation of *Beclin*-1 resulted in statistically significant protection from IM+TIC-mediated death in LN71 glioma cells (Figures 4E, S3G, and S3H). Congruently, downregulation of ATG-7 in LN71 cells also interfered with the IM+TIC-induced death (Figures 4E, 4G, and S3G–S3I). Moreover, shRNA-mediated downregulation of both *Beclin*-1 and *ATG-7* impeded the IM+TIC-mediated induction of p62/SQSTM1 degradation (Figure 4F). These results strengthen the conclusion that the cell death elicited by IM+TIC is a consequence of elevated (and not reduced) rates of autophagy.

To further characterize the status of autophagic flux in IM+TIC-treated cells, we performed transmission electron microscopy analysis (EM) of glioma cell lines LN71 and LN229 treated with vehicle control or IM+TIC for 6 or 18 hours. We observed an increase in cellular lysosomes as well as autophagic vacuoles (AVs) following 6-hour exposure to IM+TIC. Prolonged exposure to IM+TIC did not result in additional accumulation of lysosomes, although LN71 exhibited a slight reduction in total lysosomal number; there was, however, a statistically significant increase in both early (or initial) AVs and late (degradative) AVs (AVd) (Figure 4H). Occasionally, IM+TIC treatment caused the formation of "empty" autophagosomes, presumably with fully digested contents (Figure 4H, red arrows). Taken together, our data suggest that IM+TIC treatment causes non-apoptotic cell death and accentuates autophagic flux in human glioma cell lines in vitro.

Co-treatment with IM and TIC Induces Autophagy In Vivo

Having established that combinatorial treatment of LN71 human glioma cells in vitro results in induction of autophagy and non-apoptotic cell death, we proceeded to investigate the outcome of IM+TIC treatment on cell autophagy in vivo. IM+TIC treatment of mice bearing incipient gliomas produced a significant increase in LC3-positive puncta in tumor cells compared with control-treated tumors (Figure 5A); this increase was not associated with altered expression of the *MAP1LC3* gene (data not shown). We further visualized lysosomes with anti-LAMP1 (lysosomal associated membrane protein 1) antibodies and observed an evident co-localization with LC3 dots (Figure 5B). Therefore, autolysosome formation is increased in IM+TIC-treated tumors compared with control tumors, indicative of productive autophagic flux.

(E) RT-qPCR analysis of LC3 (MAP1LC3) mRNA expression in *GRLp53fko* tumors, sham-treated or treated with IM for 72 hr (see Supplemental Information). Ns, no statistical significance by unpaired Student's t test.

(F) Representative immunoblotting of LC3 proteins in primary glioma cell cultures collected from *GRLp53het* and *GRLp53fko* animals, control or IM treated alone or in conjunction with 50 nM Baf A for 4 hr (see Supplemental Information). Quantification of LC3II levels in treated cultures relative to controls is presented below the immunoblot.

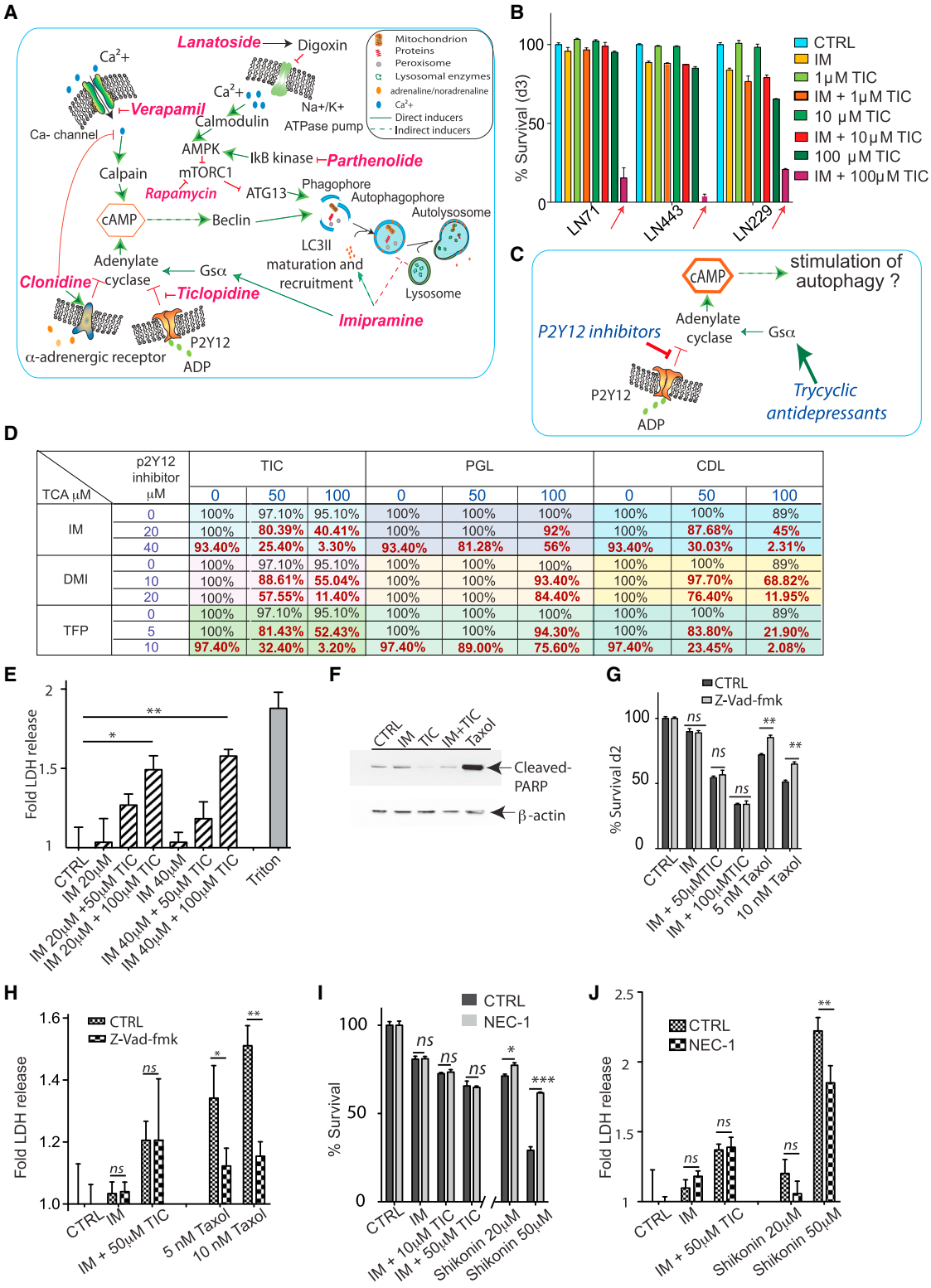

TCA μM	p2Y12 inhibitor μM	TIC 0	TIC 50	TIC 100	PGL 0	PGL 50	PGL 100	CDL 0	CDL 50	CDL 100
IM	0	100%	97.10%	95.10%	100%	100%	100%	100%	100%	89%
	20	100%	**80.39%**	**40.41%**	100%	100%	**92%**	100%	**87.68%**	**45%**
	40	**93.40%**	**25.40%**	**3.30%**	**93.40%**	**81.28%**	**56%**	**93.40%**	**30.03%**	**2.31%**
DMI	0	100%	97.10%	95.10%	100%	100%	100%	100%	100%	89%
	10	100%	**88.61%**	**55.04%**	100%	100%	**93.40%**	100%	**97.70%**	**68.82%**
	20	100%	**57.55%**	**11.40%**	100%	100%	**84.40%**	100%	**76.40%**	**11.95%**
TFP	0	100%	97.10%	95.10%	100%	100%	100%	100%	100%	89%
	5	100%	**81.43%**	**52.43%**	100%	100%	**94.30%**	100%	**83.80%**	**21.90%**
	10	**97.40%**	**32.40%**	**3.20%**	**97.40%**	**89.00%**	**75.60%**	**97.40%**	**23.45%**	**2.08%**

Figure 3. TIC Synergizes with IM in Promoting Death in Cultured Mouse and Human Glioma Cells

(A) Schematic representation of the proposed regulation of cell autophagy by different clinically approved drugs. The agents used were either identified using cell-based screens (Hundeshagen et al., 2011; Williams et al., 2008) or were previously established to be modulators of autophagy (for references, see Table S1). Six drugs (highlighted in pink font) targeting different nodes in this circuit were tested, alone and in combination with IM (see Figure S2).

(legend continued on next page)

To further investigate the effects of increased autophagic flux in the IM+TIC-treated tumors, we performed a morphological analysis by EM. We found that 9.5 ± 4.6% of the IM+TIC-treated glioma cells in vivo exhibited features of autophagy-associated cell death (AACD) (as defined by (Tasdemir et al., 2009; Petrini et al., 2012; Tinari et al., 2008) (Figure 5C). Namely, the dying cancer cells contained intact nuclei and had increased vacuolization, reduced numbers of cellular organelles, and increases in the number and size of AVs (Figure 5D) and in the size of AVd (Figure S4A).

We next sought to functionally connect autophagy with the effects of IM+TIC treatment on gliomas in vivo. LN229 glioma cells were engineered with an ATG7 shRNA lentiviral vector to have reduced expression of ATG7 (described in Supplemental Information). As presented in Figures 5E and 5F and Figure S4B, the ATG7 knockdown obviated the tumor growth inhibition and survival benefit elicited by IM+TIC, indicating that the autophagic regulatory circuit was important for the therapeutic effects of these agents.

The Combination of IM and TIC Has Therapeutic Benefit in Multiple Models of Glioma In Vivo

To further assess the therapeutic potential of IM+TIC in gliomas, we evaluated the efficacy of the combination in mice bearing de novo tumors. *GRLp53het* and *GRLp53fko* mice with asymptomatic incipient neoplasias were identified as described earlier, stratified into cohorts, and subjected to IM, TIC, or IM+TIC treatment (5 days/week) until a defined endpoint 13 weeks later, or until tumor progression dictated cessation. The IM+TIC treatment resulted in a significant survival advantage over either mono-therapy for both *GRLp53het* (59% GBM-like and 29% AA at end stage) and *GRLp53fko* (80% GBM-like at end stage) animals, without appreciable toxicity (Figures 5G and 5H). Greater than 50% of the *GRLp53het* animals survived more than 90 days following the identification of lesions, compared with 13 days in the control group (Figure 5G). The end-stage tumors in the IM+TIC-treated cohort had lower grade malignancy compared with both control cohorts and animals subjected to IM and TIC mono-therapy. The treatment also extended the median survival of *GRLp53fko* late-stage tumor-bearing animals, from 14–36 days in the IM+TIC-treated group (Figure 5H). The IM+TIC-treated *GRLp53fko* mice also had a higher percentage of lower grade (II and III) tumors compared with both the control group and animals treated with IM or TIC mono-therapy (Figure 5H). We further substantiated the therapeutic potential of IM+TIC treatment in vivo in an alternative model of gliomagenesis, *GNLp53fko*, elicited by the targeted deletion of the NF1 tumor suppressor gene that is implicated in a subclass of human glioma (Supplemental Information and Figures S4C and S4D). In this model, the survival of late-stage tumor-bearing mice treated with IM+TIC was 23.8 ± 3.7 days, compared with 5 ± 1.1 days in the control group (Figure S4E).

IM+TIC treatment was also beneficial when applied during the terminal stage of disease progression, when animals were exhibiting signs of neurological distress due to tumor burden. The mean survival of the IM+TIC treated animals was improved compared with the control group from 2.4–5.7 days while either IM or TIC mono-therapy was inefficacious (Figure 5I). The IM+TIC-treated tumors exhibited the reduction of cancer cell proliferation (Figure 5J). Thus, autophagy-promoting IM+TIC therapy is capable of slowing the rapid progression of late-stage disease. In notable contrast, inhibition of autophagy by CQ did not impart any survival advantage during analogous end-stage therapeutic trials (Figure S4F), further supporting the consensus of the data that IM+TIC is elevating autophagy to a cell-lethal level.

We further generated a syngeneic transplantable mouse model of glioma (Supplemental Information and Figures S4G and S4H), involving orthotopic inoculation of 5×10^5 of primary glioma cells derived from an end-stage *GRLp53het* mouse. Three days after transplantation, recipient animals were stratified into groups and mock-treated or treated with IM, TIC, or IM+TIC 5 days a week for 10 weeks or until the tumor burden required euthanasia. The animals treated with IM+TIC exhibited

(B) Survival of glioma cells subjected for 3 days to vehicle control, 40 μM IM, or increasing doses of TIC, alone or in combination with IM. Red arrows highlight the drug combination that induced cell death in all tested glioma cells. The experiment was conducted as described in the Supplemental Information. Lower doses of IM and TIC were tested (Figure 3D).

(C) A blowup from (A) highlighting the proposed mechanism of action of $P2Y_{12}$ inhibitors in combination with TCAs, which collectively accentuate the level of cell autophagy.

(D) Effects of three TCAs, alone or in combination with three $P2Y_{12}$ inhibitors, on the survival of LN71 glioma cells. The TCAs were IM, DMI, and TFP, and the $P2Y_{12}$ inhibitors were TIC, PGL, and CDL. The concentration of each agent is shown. The survival of treated cells is indicated as a percentage of the viable cells treated with vehicle control for each drug and drug combination. Significant effects of the treatments on cell survival are denoted in red font.

(E) Analysis of lactate dehydrogenase (LDH) release in supernatants of LN71 cells treated with IM and TIC in the indicated doses for the duration of three days. Results are presented as the fold increase in LDH relative to control-vehicle-treated cells. Triton X-100 (0.1%) was used as a positive control for the assay. The experiment was conducted in triplicate. *$p \leq 0.01$ and **$p \leq 0.005$ by two-tailed Student's t test.

(F) Representative immunoblot for cleaved PARP as a measure of apoptosis in LN71 cells, either control-treated or treated for 24 hr with 40 μM IM, 100 μM TIC, or IM+TIC. Taxol (100 nM for 24 hr) served as a positive control for induction of apoptosis. Beta-actin was used as a loading control.

(G) Survival of LN71 cells treated for 48 hr with vehicle control, 40 μM IM alone, or IM+TIC, with or without the pan-caspase inhibitor z-Vad(OMe)-fmk (50 μM). The apoptosis-inducing agent Taxol was used to illustrate zVad(Ome)-fmk activity. The experiment was conducted as described in the Supplemental Information. **$p \leq 0.005$. *ns*, no statistically significant difference by a two-tailed Student's t test.

(H) LDH release into supernatants of LN71 cells treated as in (G). *$p \leq 0.05$ and **$p \leq 0.005$. *ns*, no statistically significant difference by a two-tailed Student's t test.

(I) Survival of LN71 cells subjected treated for 24 hr with vehicle control, 40 μM IM alone, or IM+TIC, with or without the RIPK1 inhibitor necrostatin-1 (Nec-1) (25 μM). The necrosis-inducing agent shikonin (Huang et al., 2013) was used to document Nec-1 activity. The experiment was conducted as described in the Supplemental Information. *Ns*, no statistically significant difference. *$p = 0.02$ and ***$p < 0.005$, analyzed by a two-tailed Student's t test.

(J) LDH release into supernatants of LN71 cells treated as in (I). **$p \leq 0.01$. *ns*, no statistically significant difference by a two-tailed Student's t test.

See also Figure S2 and Table S1.

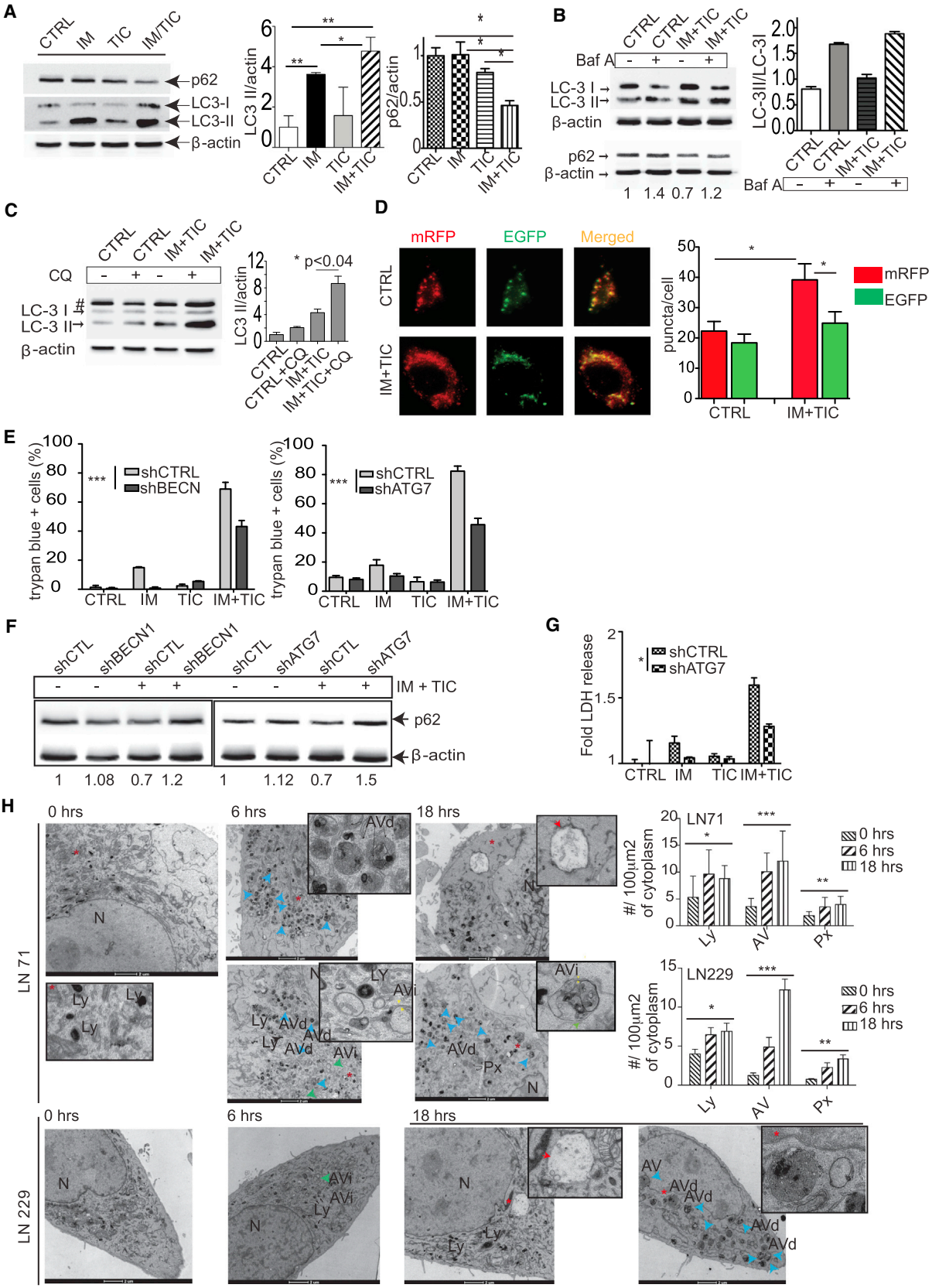

(legend on next page)

prolonged overall survival compared with the control cohort (Figure S4I).

As described above, the IM+TIC combination also reduced the growth of subcutaneous (s.c.) transplanted LN229 glial tumors (Figures 5E and 5F). To substantiate this result in the context of the CNS microenvironment, we established an orthotopic transplant model of human GBM (described in Experimental Procedures). Four days after transplantation with LN229 cells, the animals were stratified into cohorts and treated as described above. IM+TIC treatment extended survival of the tumor-bearing animals from 51 days' median survival in the control group to 61 days in the treated cohort (Figure S4J). In contrast, IM and TIC as single agents had no demonstrable effect in prolonging the survival of animals bearing aggressive transplanted tumors of mouse or human origin (Figures S4K and S4L). IM+TIC also elicited changes in tumor histopathology. The treated tumors contained large areas of tissue necrosis and displayed reduced cellularity compared with control tumors (Figure S4M).

IM and TIC Coordinately Upregulate cAMP Levels in Gliomas

A number of studies implicate cAMP in the induction of autophagy (Mestre and Colombo, 2012; Ugland et al., 2011) (Figure 3A). TCAs and $P2Y_{12}$ inhibitors are suggested to upregulate cAMP levels in the cell by distinct mechanisms (Defreyn et al., 1991; Donati and Rasenick, 2005). To determine whether the observed synergistic effects of the IM+TIC treatment on survival and histopathology are mediated by modulation of cAMP levels in gliomas, we analyzed cAMP concentrations in *GRLp53fko* tumors untreated or treated with each agent alone or in combination. The 3-day treatment of animals with IM and TIC as monotherapy did not affect cAMP levels in tumors, whereas IM+TIC increased cAMP levels in the tumor tissue (Figure 6A). Similarly, although neither agent alone affected cAMP levels in glioma cell lines, IM+TIC treatment increased cAMP levels when adjusted to total protein concentration (Figure 6B).

The cAMP signaling circuit involves a number of downstream effectors, including PKA and CREB, and the recently described EPAC-1/2 (for review, see Gloerich and Bos, 2010) (Figure 6C). Both branches of the cAMP circuit are known to regulate the ERK-signaling pathway (Ster et al., 2007; Vossler et al., 1997), activation of which can in turn lead to an increase in autophagic flux (Ugland et al., 2011). A number of cAMP analogs with different specificities for these effectors have been characterized (Christensen et al., 2003) (Figure 6C). To determine if the activated cAMP signaling circuitry is involved in the reduced survival of IM- and IM+TIC-treated glioma cells, we first tested a cAMP analog, *Dibutyryl-cAMP* (dbcAMP), which has high specificity for PKA (Christensen et al., 2003), alone and in combination with IM or TIC in LN71 cells. The co-treatment of cells with IM or TIC in the context of ectopically increased levels of dbcAMP had no impact on glioma cell survival (Figure 6D). Congruent with this observation, the PKA-specific inhibitor KT5720 had little effect on IM+TIC-mediated death in vitro. We also did not observe increased phosphorylation levels of PKA targets in response to IM+TIC (Figure S5).

In contrast, perturbation of the EPAC branch had a discernible effect. A non-hydrolyzable cAMP analog, 8-CPT-cAMP, which selectively activates EPAC, and a highly specific EPAC agonist, 8-CPT-Me-cAMP-AC (Vliem et al., 2008), both intensified the IM- and TIC-mediated cell death in glioma cells (Figures 6E and 6F). Conversely, shRNA-mediated downregulation of EPAC1 levels using two different shRNAs partially blocked the IM+TIC-induced cell death in gliomas (Figures 6G–6J). In light of these results, we conclude that elevating cAMP levels by combining TCAs and inhibitors of purinergic receptor $P2RY_{12}$ (Figure 7) is retarding gliomagenesis. Consequently, we establish the importance of this pathway in malignant brain tumor progression as suggested by epidemiological analysis in the case of TCAs

Figure 4. The Combination of IM+TIC Increases Autophagic Flux In Vitro

(A) Representative immunoblot for p62 and LC3 protein expression in LN71 cells, control or treated for 24 hr with 40 μM IM, 100 μM TIC, or IM+TIC (see Supplemental Information). *$p < 0.05$ and **$p < 0.02$ by unpaired Student's t test.

(B) Representative immunoblotting of p62 and LC3 proteins in LN71 cell cultures, control or IM+TIC treated, alone or in conjunction with 100 nM of Bafilomycin A (Baf A), for 4 hr (see Supplemental Information). Quantification of levels in treated cultures relative to controls is presented to the right (LC3-II/LC3-I) and below (p62) the immunoblot.

(C) Representative immunoblot of LC3 proteins in LN71 cells, control or treated for 24 hr with 40 μM IM + 100 μM TIC, followed or not with 10 μM CQ added 2 hr after IM+TIC. #Non-specific band. *$p < 0.04$ by unpaired Student's t test.

(D) Analysis of autophagosomes ($EFGP^+$ and $mRFP^+$) and autolysosomes ($mRFP^+$ only, because EGFP is degraded) using the ptfLC3 reporter transfected into LN71 cells, control or treated for 48 hr with 40 μM IM + 50 μM TIC. On the right, quantification of $mRFP^+$ and $EGFP^+$ puncta. *$p < 0.04$ by unpaired Student's t test.

(E) Survival of LN71 glioma treated for 2 days with 40 μM IM, 50 μM TIC, or IM+TIC, with or without knockdown of BECN1 (sh550) (left) or ATG7 (sh 7587) (right) determined by trypan blue exclusion method. ***$p \leq 0.001$ determined by two-way ANOVA.

(F) Representative immunoblotting analysis for p62 protein expression in LN71 cells infected with vectors expressing shBECN1 (sh550), shATG-7 (sh7587), or CTRL shRNA (LO.1) treated for 24 hr with IM+TIC or sham control (see Supplemental Information). p62 expression in cells expressing control shRNA is assigned a value of 1.

(G) Analysis of LDH release in supernatants of LN71 transfected with control shRNA vector (shCTRL) or shATG-7 (sh7587), each treated with 40 μM IM, 50 μM TIC, or IM+TIC for 3 days. The results are presented as the fold increase in LDH relative to control-vehicle-treated cells. The experiment was conducted in triplicate. *$p \leq 0.05$ by a two-tailed Student's t test.

(H) Representative EM images of LN71 and LN229 cells, control or treated for 6 or 18 hr with the IM+TIC combination. The red asterisks indicate the area of the images represented in the magnified insets. Cellular organelles were identified as described in the Supplemental Information. AVi, initial AVs (green arrows); Avd, late or degradative AVs (blue arrows); Ly, lysosomes; N, nucleus; Px, peroxisomes. The yellow arrows show double membranes in autophagosomes. Red arrows point to "empty" autophagolysosomes. Analysis was performed according to published guidelines (Eskelinen, 2008). The scale bars represent 2 μm. Quantification of cellular Ly, AV, and Px in LN71 and LN229 cells, control or IM+TIC treated, is presented to the right. *$p \leq 0.05$, **$p \leq 0.01$, and ***$p \leq 0.0001$ by one-way ANOVA. The analysis was performed in triplicate. At least 14 independent images were considered.

See also Figure S3.

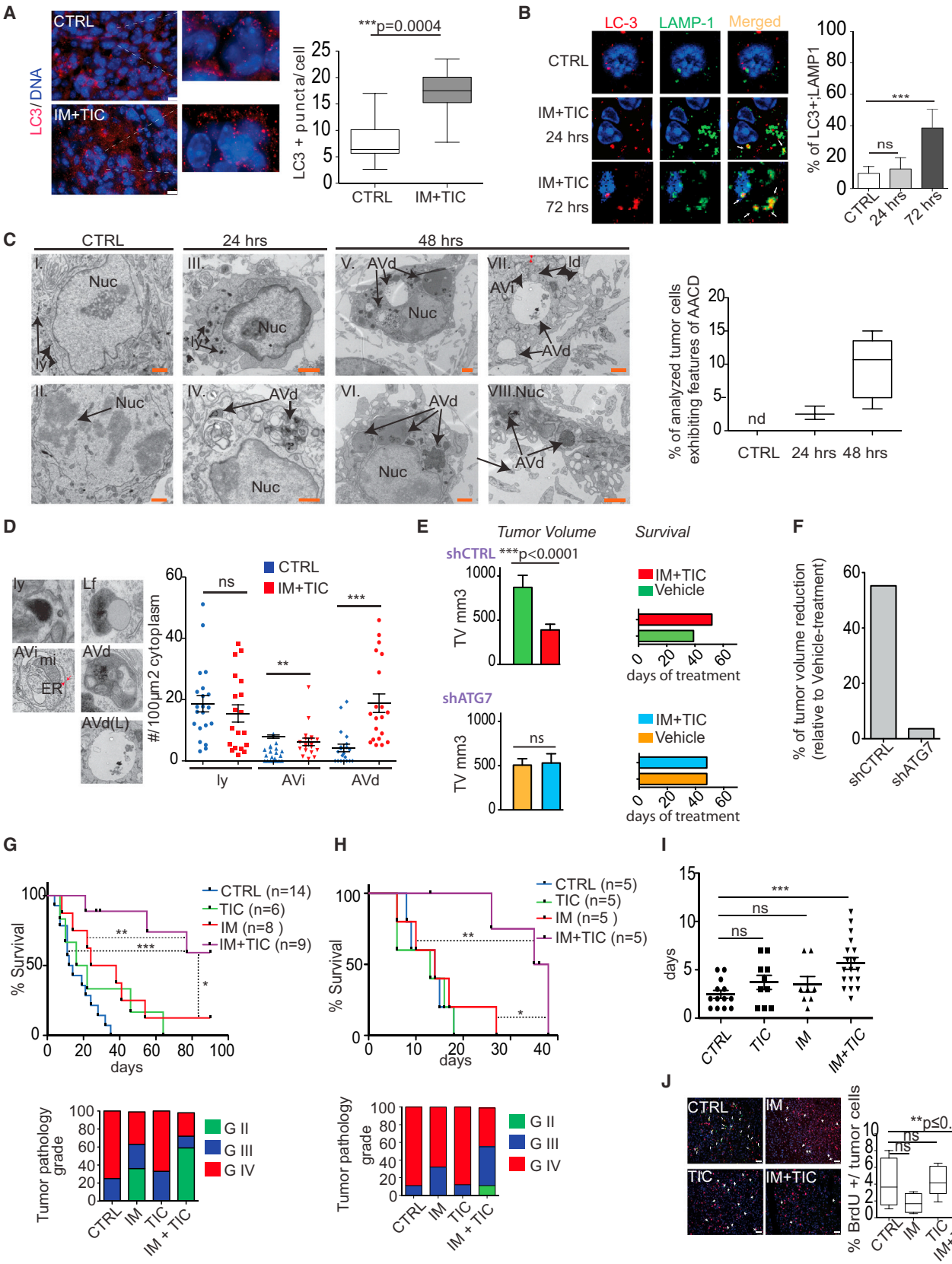

(legend on next page)

(Walker et al., 2011) and association with elevated expression for $P2RY_{12}$ (Figure S6).

DISCUSSION

In this study, we assessed the hypothesis that perturbation of autophagy could have a deleterious effect on glioma progression, motivated both by an epidemiological study suggesting that chronically depressed patients being treated long term with TCAs had a reduced incidence of glioma (Walker et al., 2011) and by experimental evidence that one such agent, IM, modulated autophagy of glioma cells in culture (Jeon et al., 2011). Because IM mono-therapy only modestly prolongs the survival of tumor-bearing animals, we hypothesized that combining IM with other agents known to potentiate autophagy at distinctive nodes in the autophagic regulatory circuit might increase its therapeutic benefit. Among six such drugs tested in a screen of human GBM cell lines, only TIC, an antiplatelet agent targeting the purinergic receptor $P2Y_{12}$ ($P2RY_{12}$), exhibited a synergistic effect with IM in impairing cell survival.

Although $P2RY_{12}$ is not reported to be highly expressed in normal tissues other than platelets and glia (Hollopeter et al., 2001), it is upregulated in different types of human tumors and appears to be associated with poor prognosis for patients with glioma, colon, and non-small-cell lung cancer (NSCLC) (Figure S6). Unconventional roles for purinergic receptors in cancer progression are beginning to be explored (Di Virgilio, 2012). Here we present evidence that $P2RY_{12}$ inhibitors, although inefficacious as mono-therapy in glioma, can synergize with three different TCAs, markedly elevating cell death. Although treatment with a prototypical TCA and a $P2Y_{12}$ inhibitor (IM and TIC, respectively) exhibits therapeutic benefits in several distinctive mouse models of glioma, the question of whether all human GBMs will be similarly responsive remains open, recognizing their heterogeneity and the diversity of driver mutations, including rearrangements, and amplification of the EGFR and PDGFR genes. Therefore, it will be important in future studies to assess IM+TIC therapy alone and in combination with therapies targeting distinct driver mutations in the broader genetic landscape of glioma.

The experimental evidence congruently supports the interpretation that IM+TIC accentuates autophagy by coordinately elevating the level of cAMP. The importance of cAMP signaling in gliomas has been highlighted in several studies. Thus, CXCL12- or phosphodiesterase 4A1-mediated reduction in cAMP levels in the brain promotes gliomagenesis following the loss of NF1 (Warrington et al., 2007, 2010). Conversely, reactivation of cAMP signaling, or exposure of glioma cells to cAMP analogs, inhibits growth of xenografted brain tumors or decreases proliferation and survival of glioma cells in vitro (Goldhoff et al., 2008; Hill et al., 2009; Sugimoto et al., 2013; Yang et al., 2007). We now describe an alternative mechanism of increasing cAMP levels in gliomas with a combination of FDA-approved agents that elicit elevated rates of autophagy, with therapeutic benefit. Our data suggest that although the PKA branch of the cAMP signaling circuit is dispensable for this process, the EPAC-branch mediates the cellular response to IM+TIC. Collectively, our data indicate that IM+TIC increases cAMP levels in the cell, which, via the EPAC branch of the cAMP signaling cascade, induces AACD in glioma cells (Figure 7). Notably, we exclude

Figure 5. Combined Treatment with IM+TIC Elevates Autophagy and Prolongs Survival of Mice with Brain Tumors

(A) Representative IHC analysis of LC-3 expression in tumors collected from tumor-bearing *GRLp53fko* animals treated with vehicle (CTRL) or IM (40 mg/kg/day) + TIC (1 mg/kg/day) daily for 72 hr (see Supplemental Information). The scale bars represent 10 μm. Graph shows the quantification of LC3 in tumors (puncta per cell). Data are presented as mean ± SEM. Statistical analysis was performed using the unpaired Student's t test.

(B) Intracellular localization of LC-3 and the lysosomal marker LAMP1 in tumors, either vehicle control (CTRL) or treated with IM+TIC for 24 and 72 hr, determined by confocal microscopy (see Supplemental Information). The graph presents LC3 and LAMP1 co-localization as a percentage of total LAMP1 dots. ***$p < 0.0001$. ns, no statistical significance by a two-tailed Student's t test.

(C) Representative EM images of *GRLp53fko* tumors treated either with vehicle control (I, II) or with IM+TIC for 24 hr (III, IV) or 48 hr (V–VIII). For organelle definition and experimental details, see Supplemental Information. The scale bars represent 1 μm. IM+TIC-treated tumors show different stages of AACD (V–VIII), characterized by cell shrinkage, extensive vacuolization, and depletion of organelles. Graph shows the quantitative analysis of tumor cells exhibiting the features of AACD, presented as percentage of cells showing this features in ultrathin sections. At least 22 independent images per section were analyzed. nd, not detected.

(D) Exemplary images of organelles identified in *GRLp53fko* tumors. AVd (L), late degradative AV; ER, endoplasmic reticulum; Lf, lipofuscin; Mi, mitochondrion. (Note the typical double membrane [red arrows] characterizing AVi.) To the right is a quantification of cellular organelles in *GRLp53fko* tumors, control and treated for 48 hr with IM+TIC, per 100 μm^2 cytoplasm. At least 20 cell bodies with clearly visible nuclei were considered for each treatment. ns, no statistical significance. **$p < 0.005$ and ***$p < 0.0001$ by a two-tailed Student's t test.

(E) Effects of vehicle control or IM+TIC treatment on tumor volumes (left column) or survival (right column) of s.c. xenografts from LN229 cells infected with shRNA control (shCTRL) or shATG7. Tumor volumes were determined at a defined endpoint of 39 days, when control mice were at end stage (left). Survival was determined when the average tumor volume of each cohort reached end stage, approximately 870 mm^3 (right). ***$p < 0.0001$. ns, no statistical significance by a two-tailed Student's t test.

(F) Therapeutic potential of IM+TIC treatment presented as the reduction in the average tumor volume of s.c. xenografts from LN229 cells described above, calculated when tumors from vehicle-treated mice reached an average size of 870 mm^3.

(G) Survival of tumor-bearing *GRLp53het* animals subjected to the indicated treatments initiated 24 hr after tumor detection (Supplemental Information). n = cohort size. ***$p < 0.0001$, **$p < 0.005$, and *$p \leq 0.02$ by the Mantel-Cox test. The graph below shows the distribution of tumor grade (G) in end-stage *GRLp53het* animals; see the Supplemental Information for grading metrics.

(H) Survival of tumor-bearing *GRLp53fko* animals subjected to the indicated treatments initiated 24 hr after tumor detection (Supplemental Information). *$p < 0.02$ and **$p \leq 0.005$ by the Mantel-Cox test. n = number of animals per cohort. The distribution of tumor grade (G) in end-stage *GRLp53fko* animals is shown below.

(I) Scatterplot shows the survival of symptomatic (end-stage) tumor-bearing animals following enrollment into trials. Data are represented as mean (±SEM). n = cohort size. ***$p < 0.001$. ns, no statistical significance by a two-tailed Student's t test.

(J) IHC analysis of cell proliferation assayed by Ki67 expression (shown) and BrdU incorporation (not shown) in the tumor samples from the cohorts analyzed in (I) (see Supplemental Information for methods). The scale bars represent 50 μm. Quantification of BrdU-positive cells is presented to the right. ns, no statistical significance by a two-tailed Student's t test.

See also Figure S4.

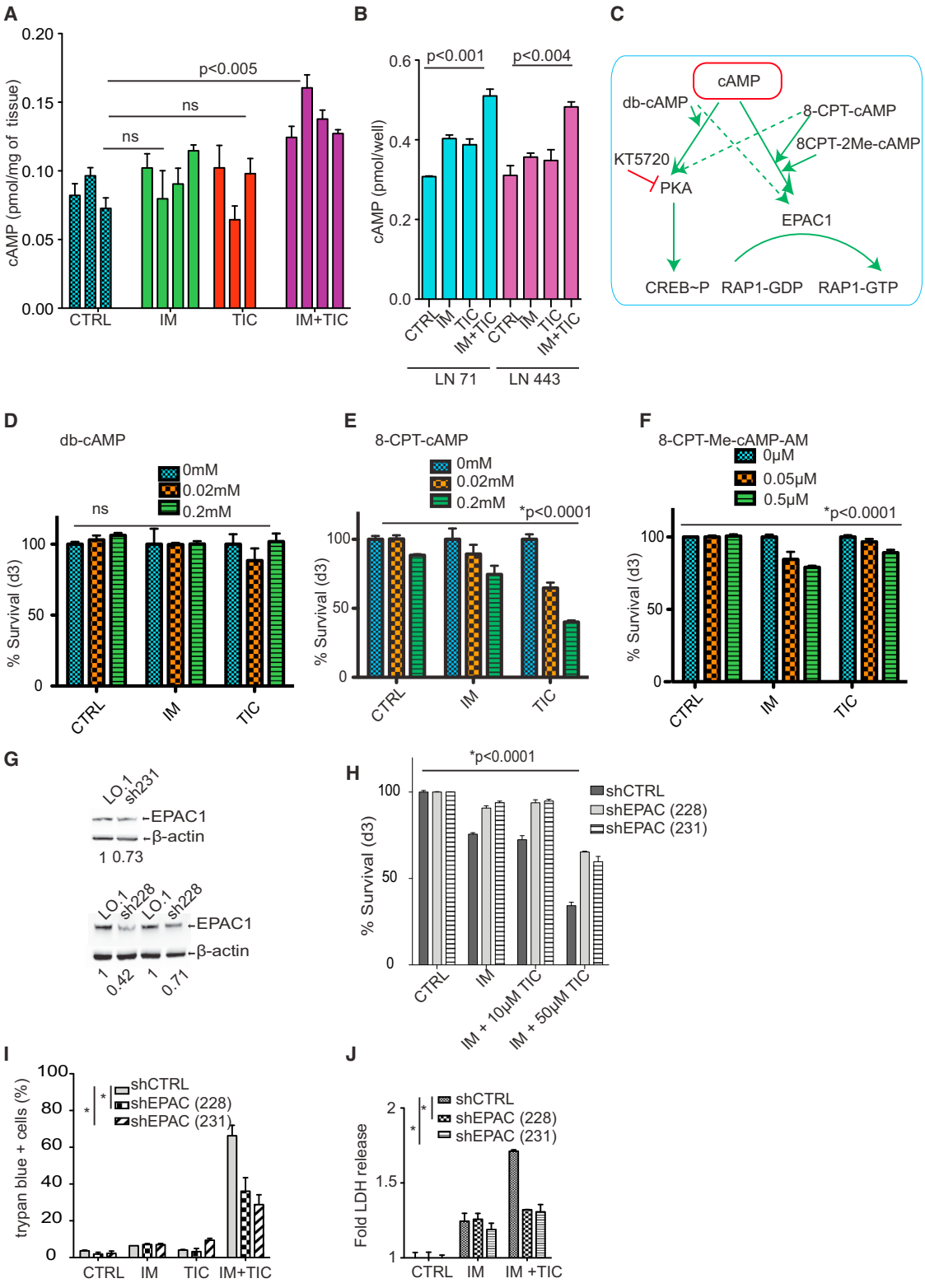

Figure 6. Dual Treatment with IM+TIC Elevates cAMP Levels in Gliomas

(A) cAMP levels in tumor tissue adjusted to tumor weight. CTRL, vehicle-treated tumor-bearing animals; IM, TIC, and IM+TIC, tumor-bearing animals treated daily for 3 days (Supplemental Information). At least three animals per condition were analyzed. The analysis was performed in triplicate. Statistical analysis used two-way ANOVA.

(legend continued on next page)

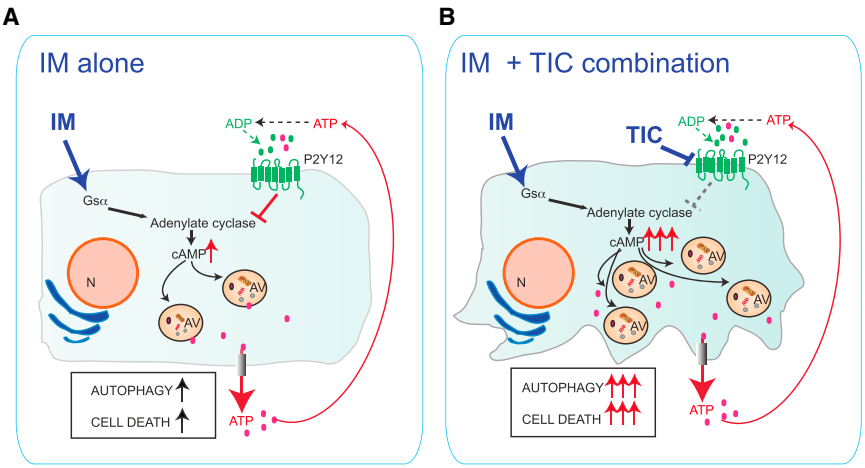

Figure 7. Schematic of the Proposed Mechanisms Underlying the Synergistic Effects of IM+TIC on the Induction of AACD through Elevated cAMP Signaling

(A) IM treatment activates adenylate cyclase and induces cAMP-mediated autophagy. Autophagic cells release ATP (Ayna et al., 2012). Extracellular ATP is rapidly degraded into ADP and other ATP metabolites. ATP and ADP can activate the purinergic receptor $P2Y_{12}$, triggering feedback inhibition of adenylate cyclase activity, thereby attenuating cAMP-mediated autophagy so as to ameliorate excessive autophagy that can otherwise result in AACD. Gsα, G protein subunit alpha. (B) Combined exposure of cells to IM and the $P2Y_{12}$ inhibitor TIC short-circuits the ADP/ATP-induced feedback inhibition of adenylate cyclase, which increases cAMP levels, eliciting hyperactivated autophagy and consequent cell death. See also Figure S6.

apoptosis and necroptosis as mediators of cell death in response to these agents and functionally associate autophagy. In contrast, TCAs have been shown to enhance apoptosis and impair tumor growth in a mouse model of lung cancer (Jahchan et al., 2013). Although autophagy was not assessed in this study, the result suggests there may be context-dependent effects of TCAs in different tumors types, warranting further investigation.

The role of autophagy in cancer progression is complex. The outcome of autophagy activation in cancer cells depends on the stage of the disease progression, cell type, oncogenic drivers, and the intensity of the activating signal (White, 2012). For example, in some instances, pharmacological induction of autophagy can be cytoprotective, whereas subsequent inhibition of autophagy by lysosomotropic agents can result in apoptosis (Fan et al., 2010). On the other hand, increasing evidence suggests that some anticancer agents promote AACD and that inhibition of autophagy under these conditions reduces their cytotoxicity (for review, see Eberhart, 2014).

It is currently believed that AACD is the result of excessive rates of autophagic flux this is distinct from death by apoptosis or necroptosis (Mariño et al., 2014). Recently a panel of experts in the field of cell death suggested the following criteria to define AACD: (1) increased autophagic flux, (2) cell death without the evident involvement of apoptosis, and (3) genetic inhibition of autophagy by at least two regulatory factors suppresses the cell killing (Galluzzi et al., 2012). The IM+TIC-mediated cell death in vitro meets all the proposed requirements.

The tumor-inhibiting role of autophagy in certain human cancers is increasingly being demonstrated (Aita et al., 1999). For example, in GBM patients, comparatively higher levels of autophagy are associated with better survival prognosis (Aoki et al., 2008). Increased autophagic flux was recently shown to impair tumor growth of NSCLC in mice (Xia et al., 2014), whereas inhibition of autophagy by hydroxychloroquine accelerated tumor formation in a model of pancreatic ductal adenocarcinoma (Rosenfeldt et al., 2013). These results are all consistent with the hypothesis that excessive autophagy can be tumor suppressive. Our data add glioma to this growing list.

Aside from surgical removal, which is often not possible because of tumor location and infiltration, the current conventional therapy for glioma patients consists of ionizing irradiation alone or in combination with the DNA alkalyting agent temozolomide (Hegi et al., 2005; Stupp et al., 2005). Each of these therapies elicits an increase in autophagic flux. A compelling body of data obtained in vitro suggests that the observed autophagy is enhancing therapeutic modalities by evoking AACD in cells resistant to apoptosis (reviewed by Palumbo and Comincini, 2013). We now show that the use of agents that enhance AACD reduces survival of glioma cells in vitro and restrains glioma progression. It is reasonable to suggest that incorporation of IM+TIC might enhance the therapeutic benefit of conventional treatments for gliomas, and we are currently investigating this possibility.

In summary, we describe the successful application of two FDA-approved pharmacological agents to target glioma cell

(B) cAMP levels in human glioma cell lines LN71 and LN443, control or treated with IM (40 μM), TIC (100 μM), or IM+TIC for 24 hr, adjusted to total protein concentration. The analysis was in triplicate and assessed by two-way ANOVA.
(C) A schematic representation of cAMP signaling cascade, illustrating where the PKA inhibitor KT5720 and several cAMP analogs are proposed to act on the different branches of the cAMP pathway.
(D–F) Survival of LN71 cells treated for three days with vehicle, IM, or TIC alone, or in combination with cAMP analogs: dbcAMP (D), 8-CPT-cAMP (E), and 8-CPT-Me-cAMP-AC (F) in indicated concentrations. Statistical analysis was performed by two-way ANOVA.
(G) Representative immunoblotting analysis for EPAC1 protein expression in LN71 glioma cell lines infected with lentiviral vectors expressing shEPAC1 (sh231 and sh228) or control shRNA (LO.1) cells. (Procedures are described in the Supplemental Information.)
(H) Survival of LN71 glioma cells, with or without knockdown of EPAC, subjected for 3 days to treatment with 40 μM IM alone or in conjunction with TIC, analyzed with the Cell Titer GloR (see Supplemental Information). *$p < 0.0001$ by two-way ANOVA.
(I) Survival of LN71 cells described and treated as in (G) and (H) analyzed by the trypan blue exclusion method. *$p < 0.0001$ by two-way ANOVA.
(J) Survival of LN71 cells described in (G), assessed by the LDH release method following exposure for 72 hr to IM and IM+TIC. *$p < 0.0001$ by two-way ANOVA.
See also Figure S5.

survival and malignant progression by eliciting AACD via induction of the cAMP-signaling pathway. Notably, other analyzed inhibitors of the $P2RY_{12}$ receptor, such as CDL or PGL, may prove applicable to this mechanism-based therapeutic targeting, as might other TCAs, affording flexibility in identifying combinations with the best efficacy and toxicity profiles in humans.

The results presented herein offer a provocative strategy to target apoptosis-resistant brain tumors by hyperactivating levels of cellular autophagy; such dual targeting of autophagy with repurposed, pharmacologically tractable drugs may warrant consideration for clinical trials.

EXPERIMENTAL PROCEDURES

Mouse Models and Bioluminescent Monitoring

Mice were housed, fed, and treated in accordance with protocols approved by the committee for animal research of Canton Vaud, Switzerland. The de novo and orthotopic models and manipulations are described in detail in Supplemental Experimental Procedures.

Luminescent images were obtained 5 min after injections of firefly D-luciferin, potassium salt (L-8220; Biosynth) using an IVIS-100 Imaging System (PerkinElmer) at field view D with the following parameters: 1 min exposure, small binning, F/stop 1, emission filter open. The images were analyzed with the Living Image 3.2 Analysis software package (Caliper, PerkinElmer). The data were expressed as total photon flux (photons per second). Mice whose tumor burden produced 3.5×10^6 to 4.5×10^6 photons per second in square centimeters in regions of interest were enrolled into therapeutic trials (see Figures 1A, 1E, 5G, and 5H).

Immunoblotting, Histology and Immuno-histology, Cell Culture, and Transmission EM

These procedures were performed as described by Shchors et al. (2013) and in the Supplemental Information.

cAMP Measurement

cAMP was measured by competitive immunoassay using the cAMP Direct Immunoassay Kit (K371-100; BioVision) according to the manufacturer's instructions, as described in the Supplemental Information.

Statistical Analysis and Quantification of Immune Staining

Data are presented as mean ± SEM from at least three independent experiments, unless indicated otherwise. Kaplan-Meier survival curves were generated using GraphPad Prism 5. The statistical analysis of the survival curves was done according to the Mantel-Cox test. The quantification of tumor proliferation and apoptosis was performed using the Fiji software package (http://rsb.info.nih.gov/ij).

SUPPLEMENTAL INFORMATION

Supplemental Information includes Supplemental Experimental Procedures, six figures, and one table and can be found with this article online at http://dx.doi.org/10.1016/j.ccell.2015.08.012.

AUTHOR CONTRIBUTIONS

D.H. and K.S. designed the experiments and analyzed the data. K.S. and A.M. performed the experiments. D.H. and K.S. wrote the manuscript. All authors agree with the conclusions presented in the manuscript.

ACKNOWLEDGMENTS

This work was supported by grants from Fondation S.A.N.T.É. and the School of Life Sciences at EPFL. We thank M. Hegi (Department of Neuro-oncology, Centre Hospitalier Universitaire Vaudois) for providing the *LN* series of human GBM cultures. We are grateful to P.Y. Dietrich (University Hospital Geneva), P.S. Mischel (University of California, San Diego, and Ludwig Institute for Cancer Research), and Jeffrey A. Kasten (École Polytechnique Fédérale de Lausanne [EPFL]) for valuable comments on the manuscript. Special thanks to members of the Hanahan laboratory for valuable discussions. We further acknowledge G. Knott, S. Rosset, and M. Croisier in the BioEM Facility, EPFL, for EM, as well as the Bioimaging & Optics Platform (PT-*BIOP*) and the Histology Core Facility at EPFL for their services. We thank G. Romain for help defining an algorithm for quantification of LC3 puncta.

Received: November 10, 2014
Revised: April 13, 2015
Accepted: August 31, 2015
Published: September 24, 2015

REFERENCES

Aita, V.M., Liang, X.H., Murty, V.V., Pincus, D.L., Yu, W., Cayanis, E., Kalachikov, S., Gilliam, T.C., and Levine, B. (1999). Cloning and genomic organization of beclin 1, a candidate tumor suppressor gene on chromosome 17q21. Genomics *59*, 59–65.

Aoki, H., Kondo, Y., Aldape, K., Yamamoto, A., Iwado, E., Yokoyama, T., Hollingsworth, E.F., Kobayashi, R., Hess, K., Shinojima, N., et al. (2008). Monitoring autophagy in glioblastoma with antibody against isoform B of human microtubule-associated protein 1 light chain 3. Autophagy *4*, 467–475.

Ashoor, R., Yafawi, R., Jessen, B., and Lu, S. (2013). The contribution of lysosomotropism to autophagy perturbation. PLoS ONE *8*, e82481.

Ayna, G., Krysko, D.V., Kaczmarek, A., Petrovski, G., Vandenabeele, P., and Fésüs, L. (2012). ATP release from dying autophagic cells and their phagocytosis are crucial for inflammasome activation in macrophages. PLoS ONE *7*, e40069.

Barańska, J., Czajkowski, R., and Sabała, P. (2004). Cross-talks between nucleotide receptor-induced signaling pathways in serum-deprived and non-starved glioma C6 cells. Adv. Enzyme Regul. *44*, 219–232.

Bjørkøy, G., Lamark, T., Pankiv, S., Øvervatn, A., Brech, A., and Johansen, T. (2009). Monitoring autophagic degradation of p62/SQSTM1. Methods Enzymol. *452*, 181–197.

Carrasquero, L.M., Delicado, E.G., Jiménez, A.I., Pérez-Sen, R., and Miras-Portugal, M.T. (2005). Cerebellar astrocytes co-express several ADP receptors. Presence of functional P2Y(13)-like receptors. Purinergic Signal. *1*, 153–159.

Christensen, A.E., Selheim, F., de Rooij, J., Dremier, S., Schwede, F., Dao, K.K., Martinez, A., Maenhaut, C., Bos, J.L., Genieser, H.G., and Døskeland, S.O. (2003). cAMP analog mapping of Epac1 and cAMP kinase. Discriminating analogs demonstrate that Epac and cAMP kinase act synergistically to promote PC-12 cell neurite extension. J. Biol. Chem. *278*, 35394–35402.

Defreyn, G., Gachet, C., Savi, P., Driot, F., Cazenave, J.P., and Maffrand, J.P. (1991). Ticlopidine and clopidogrel (SR 25990C) selectively neutralize ADP inhibition of PGE1-activated platelet adenylate cyclase in rats and rabbits. Thromb. Haemost. *65*, 186–190.

Degterev, A., Huang, Z., Boyce, M., Li, Y., Jagtap, P., Mizushima, N., Cuny, G.D., Mitchison, T.J., Moskowitz, M.A., and Yuan, J. (2005). Chemical inhibitor of nonapoptotic cell death with therapeutic potential for ischemic brain injury. Nat. Chem. Biol. *1*, 112–119.

Di Virgilio, F. (2012). Purines, purinergic receptors, and cancer. Cancer Res. *72*, 5441–5447.

Donati, R.J., and Rasenick, M.M. (2005). Chronic antidepressant treatment prevents accumulation of gsalpha in cholesterol-rich, cytoskeletal-associated, plasma membrane domains (lipid rafts). Neuropsychopharmacology *30*, 1238–1245.

Eberhart, K. (2014). Induction of autophagic cell death by anticancer agents. In Autophagy: Cancer, Other Pathologies, Inflammation, Immunity, Infection, and Aging, M. Hayat, ed. (Academic Press), pp. 179–202.

Eskelinen, E.L. (2008). Fine structure of the autophagosome. In Methods in Molecular Biology: Autophagosome and Phagosome, V. Deretic, ed. (Humana Press), pp. 11–28.

Fan, Q.W., Cheng, C., Hackett, C., Feldman, M., Houseman, B.T., Nicolaides, T., Haas-Kogan, D., James, C.D., Oakes, S.A., Debnath, J., et al. (2010). Akt and autophagy cooperate to promote survival of drug-resistant glioma. Sci. Signal. *3*, ra81.

Friedman, H.S., Kerby, T., and Calvert, H. (2000). Temozolomide and treatment of malignant glioma. Clin. Cancer Res. *6*, 2585–2597.

Galluzzi, L., Vitale, I., Abrams, J.M., Alnemri, E.S., Baehrecke, E.H., Blagosklonny, M.V., Dawson, T.M., Dawson, V.L., El-Deiry, W.S., Fulda, S., et al. (2012). Molecular definitions of cell death subroutines: recommendations of the Nomenclature Committee on Cell Death 2012. Cell Death Differ. *19*, 107–120.

Gloerich, M., and Bos, J.L. (2010). Epac: defining a new mechanism for cAMP action. Annu. Rev. Pharmacol. Toxicol. *50*, 355–375.

Goldhoff, P., Warrington, N.M., Limbrick, D.D., Jr., Hope, A., Woerner, B.M., Jackson, E., Perry, A., Piwnica-Worms, D., and Rubin, J.B. (2008). Targeted inhibition of cyclic AMP phosphodiesterase-4 promotes brain tumor regression. Clin. Cancer Res. *14*, 7717–7725.

Hart, L.S., Cunningham, J.T., Datta, T., Dey, S., Tameire, F., Lehman, S.L., Qiu, B., Zhang, H., Cerniglia, G., Bi, M., et al. (2012). ER stress-mediated autophagy promotes Myc-dependent transformation and tumor growth. J. Clin. Invest. *122*, 4621–4634.

Hegi, M.E., Diserens, A.C., Gorlia, T., Hamou, M.F., de Tribolet, N., Weller, M., Kros, J.M., Hainfellner, J.A., Mason, W., Mariani, L., et al. (2005). MGMT gene silencing and benefit from temozolomide in glioblastoma. N. Engl. J. Med. *352*, 997–1003.

Hill, J.J., Moreno, M.J., Lam, J.C., Haqqani, A.S., and Kelly, J.F. (2009). Identification of secreted proteins regulated by cAMP in glioblastoma cells using glycopeptide capture and label-free quantification. Proteomics *9*, 535–549.

Hollopeter, G., Jantzen, H.M., Vincent, D., Li, G., England, L., Ramakrishnan, V., Yang, R.B., Nurden, P., Nurden, A., Julius, D., and Conley, P.B. (2001). Identification of the platelet ADP receptor targeted by antithrombotic drugs. Nature *409*, 202–207.

Huang, C., Luo, Y., Zhao, J., Yang, F., Zhao, H., Fan, W., and Ge, P. (2013). Shikonin kills glioma cells through necroptosis mediated by RIP-1. PLoS ONE *8*, e66326.

Hundeshagen, P., Hamacher-Brady, A., Eils, R., and Brady, N.R. (2011). Concurrent detection of autolysosome formation and lysosomal degradation by flow cytometry in a high-content screen for inducers of autophagy. BMC Biol. *9*, 38.

Jahchan, N.S., Dudley, J.T., Mazur, P.K., Flores, N., Yang, D., Palmerton, A., Zmoos, A.F., Vaka, D., Tran, K.Q., Zhou, M., et al. (2013). A drug repositioning approach identifies tricyclic antidepressants as inhibitors of small cell lung cancer and other neuroendocrine tumors. Cancer Discov. *3*, 1364–1377.

Jain, M.V., Paczulla, A.M., Klonisch, T., Dimgba, F.N., Rao, S.B., Roberg, K., Schweizer, F., Lengerke, C., Davoodpour, P., Palicharla, V.R., et al. (2013). Interconnections between apoptotic, autophagic and necrotic pathways: implications for cancer therapy development. J. Cell. Mol. Med. *17*, 12–29.

Jeon, S.H., Kim, S.H., Kim, Y., Kim, Y.S., Lim, Y., Lee, Y.H., and Shin, S.Y. (2011). The tricyclic antidepressant imipramine induces autophagic cell death in U-87MG glioma cells. Biochem. Biophys. Res. Commun. *413*, 311–317.

Kimura, S., Noda, T., and Yoshimori, T. (2007). Dissection of the autophagosome maturation process by a novel reporter protein, tandem fluorescent-tagged LC3. Autophagy *3*, 452–460.

Mariño, G., Niso-Santano, M., Baehrecke, E.H., and Kroemer, G. (2014). Self-consumption: the interplay of autophagy and apoptosis. Nat. Rev. Mol. Cell Biol. *15*, 81–94.

Marumoto, T., Tashiro, A., Friedmann-Morvinski, D., Scadeng, M., Soda, Y., Gage, F.H., and Verma, I.M. (2009). Development of a novel mouse glioma model using lentiviral vectors. Nat. Med. *15*, 110–116.

Mestre, M.B., and Colombo, M.I. (2012). cAMP and EPAC are key players in the regulation of the signal transduction pathway involved in the α-hemolysin autophagic response. PLoS Pathog. *8*, e1002664.

Mizushima, N., Yoshimori, T., and Levine, B. (2010). Methods in mammalian autophagy research. Cell *140*, 313–326.

Palumbo, S., and Comincini, S. (2013). Autophagy and ionizing radiation in tumors: the "survive or not survive" dilemma. J. Cell. Physiol. *228*, 1–8.

Pankiv, S., Clausen, T.H., Lamark, T., Brech, A., Bruun, J.A., Outzen, H., Øvervatn, A., Bjørkøy, G., and Johansen, T. (2007). p62/SQSTM1 binds directly to Atg8/LC3 to facilitate degradation of ubiquitinated protein aggregates by autophagy. J. Biol. Chem. *282*, 24131–24145.

Petersen, N.H., Olsen, O.D., Groth-Pedersen, L., Ellegaard, A.M., Bilgin, M., Redmer, S., Ostenfeld, M.S., Ulanet, D., Dovmark, T.H., Lønborg, A., et al. (2013). Transformation-associated changes in sphingolipid metabolism sensitize cells to lysosomal cell death induced by inhibitors of acid sphingomyelinase. Cancer Cell *24*, 379–393.

Petrini, I., Meltzer, P.S., Zucali, P.A., Luo, J., Lee, C., Santoro, A., Lee, H.S., Killian, K.J., Wang, Y., Tsokos, M., et al. (2012). Copy number aberrations of BCL2 and CDKN2A/B identified by array-CGH in thymic epithelial tumors. Cell Death Dis. *3*, e351.

Rosenfeldt, M.T., O'Prey, J., Morton, J.P., Nixon, C., MacKay, G., Mrowinska, A., Au, A., Rai, T.S., Zheng, L., Ridgway, R., et al. (2013). p53 status determines the role of autophagy in pancreatic tumour development. Nature *504*, 296–300.

Shannon, P., Sabha, N., Lau, N., Kamnasaran, D., Gutmann, D.H., and Guha, A. (2005). Pathological and molecular progression of astrocytomas in a GFAP:12 V-Ha-Ras mouse astrocytoma model. Am. J. Pathol. *167*, 859–867.

Shchors, K., Persson, A.I., Rostker, F., Tihan, T., Lyubynska, N., Li, N., Swigart, L.B., Berger, M.S., Hanahan, D., Weiss, W.A., and Evan, G.I. (2013). Using a preclinical mouse model of high-grade astrocytoma to optimize p53 restoration therapy. Proc. Natl. Acad. Sci. U S A *110*, E1480–E1489.

Ster, J., De Bock, F., Guérineau, N.C., Janossy, A., Barrère-Lemaire, S., Bos, J.L., Bockaert, J., and Fagni, L. (2007). Exchange protein activated by cAMP (Epac) mediates cAMP activation of p38 MAPK and modulation of Ca2+-dependent K+ channels in cerebellar neurons. Proc. Natl. Acad. Sci. U S A *104*, 2519–2524.

Stupp, R., Mason, W.P., van den Bent, M.J., Weller, M., Fisher, B., Taphoorn, M.J., Belanger, K., Brandes, A.A., Marosi, C., Bogdahn, U., et al.; European Organisation for Research and Treatment of Cancer Brain Tumor and Radiotherapy Groups; National Cancer Institute of Canada Clinical Trials Group (2005). Radiotherapy plus concomitant and adjuvant temozolomide for glioblastoma. N. Engl. J. Med. *352*, 987–996.

Sugimoto, N., Miwa, S., Tsuchiya, H., Hitomi, Y., Nakamura, H., Yachie, A., and Koizumi, S. (2013). Targeted activation of PKA and Epac promotes glioblastoma regression in vitro. Mol. Clin. Oncol. *1*, 281–285.

Tasdemir, E., Galluzzi, L., Maiuri, M.C., Criollo, A., Vitale, I., Hangen, E., Modjtahedi, N., and Kroemer, G. (2009). Methods for assessing autophagy and autophagic cell death. In Methods in Molecular Biology, V. Deretic, ed. (Humana Press), pp. 29–76.

Tinari, A., Giammarioli, A.M., Manganelli, V., Ciarlo, L., and Malorni, W. (2008). Analyzing morphological and ultrastructural features in cell death. Methods Enzymol. *442*, 1–26.

Toki, S., Donati, R.J., and Rasenick, M.M. (1999). Treatment of C6 glioma cells and rats with antidepressant drugs increases the detergent extraction of G(s alpha) from plasma membrane. J. Neurochem. *73*, 1114–1120.

Tsujimoto, Y. (2012). Multiple ways to die: non-apoptotic forms of cell death. Acta Oncol. *51*, 293–300.

Ugland, H., Naderi, S., Brech, A., Collas, P., and Blomhoff, H.K. (2011). cAMP induces autophagy via a novel pathway involving ERK, cyclin E and Beclin 1. Autophagy *7*, 1199–1211.

Vliem, M.J., Ponsioen, B., Schwede, F., Pannekoek, W.J., Riedl, J., Kooistra, M.R., Jalink, K., Genieser, H.G., Bos, J.L., and Rehmann, H. (2008). 8-pCPT-2′-O-Me-cAMP-AM: an improved Epac-selective cAMP analogue. ChemBioChem *9*, 2052–2054.

Vossler, M.R., Yao, H., York, R.D., Pan, M.G., Rim, C.S., and Stork, P.J. (1997). cAMP activates MAP kinase and Elk-1 through a B-Raf- and Rap1-dependent pathway. Cell *89*, 73–82.

Walker, A.J., Card, T., Bates, T.E., and Muir, K. (2011). Tricyclic antidepressants and the incidence of certain cancers: a study using the GPRD. Br. J. Cancer *104*, 193–197.

Walker, A.J., Grainge, M., Bates, T.E., and Card, T.R. (2012). Survival of glioma and colorectal cancer patients using tricyclic antidepressants post-diagnosis. Cancer Causes Control *23*, 1959–1964.

Warrington, N.M., Woerner, B.M., Daginakatte, G.C., Dasgupta, B., Perry, A., Gutmann, D.H., and Rubin, J.B. (2007). Spatiotemporal differences in CXCL12 expression and cyclic AMP underlie the unique pattern of optic glioma growth in neurofibromatosis type 1. Cancer Res. *67*, 8588–8595.

Warrington, N.M., Gianino, S.M., Jackson, E., Goldhoff, P., Garbow, J.R., Piwnica-Worms, D., Gutmann, D.H., and Rubin, J.B. (2010). Cyclic AMP suppression is sufficient to induce gliomagenesis in a mouse model of neurofibromatosis-1. Cancer Res. *70*, 5717–5727.

White, E. (2012). Deconvoluting the context-dependent role for autophagy in cancer. Nat. Rev. Cancer *12*, 401–410.

Williams, A., Sarkar, S., Cuddon, P., Ttofi, E.K., Saiki, S., Siddiqi, F.H., Jahreiss, L., Fleming, A., Pask, D., Goldsmith, P., et al. (2008). Novel targets for Huntington's disease in an mTOR-independent autophagy pathway. Nat. Chem. Biol. *4*, 295–305.

Xia, Y., Liu, Y.-L., Xie, Y., Zhu, W., Guerra, F., Shen, S., Yeddula, N., Fischer, W., Low, W., Zhou, X., et al. (2014). A combination therapy for Kras-driven lung adenocarcinomas using lipophilic bisphosphonates and rapamycin. Sci. Transl. Med. *6*, 263ra161.

Yang, L., Jackson, E., Woerner, B.M., Perry, A., Piwnica-Worms, D., and Rubin, J.B. (2007). Blocking CXCR4-mediated cyclic AMP suppression inhibits brain tumor growth in vivo. Cancer Res. *67*, 651–658.